Simultaneous Multi-Cation Exchange Pathway to High-Entropy Metal Sulfide Nanoparticles

Connor R. McCormick[1] and Raymond E. Schaak[1,2,3,*]

[1] *Department of Chemistry,* [2] *Department of Chemical Engineering, and* [3] *Materials Research Institute, The Pennsylvania State University, University Park, PA 16802*

ABSTRACT: High entropy materials, which contain a large number of randomly distributed elements, have unique catalytic, electrochemical, and mechanical properties. The high configurational entropy of the randomized elements drives the formation of high entropy materials, therefore high temperatures and quenching are typically required to stabilize them. Because of this, colloidal nanoparticles of high entropy materials are difficult to synthesize and remain rare, despite their desirable high surface areas and solution dispersibilities. Here, we introduce simultaneous multi-cation exchange as an alternative low-temperature pathway to colloidal nanoparticles of high entropy materials. Roxbyite $Cu_{1.8}S$ nanoparticles react with a substoichiometric mixture of Zn^{2+}, Co^{2+}, In^{3+}, and Ga^{3+} to produce nanoparticles of the high entropy metal sulfide $Zn_{0.25}Co_{0.22}Cu_{0.28}In_{0.16}Ga_{0.11}S$. The $Zn_{0.25}Co_{0.22}Cu_{0.28}In_{0.16}Ga_{0.11}S$ nanoparticles are thermally stable, and exchange reactions using fewer cations do not produce the high entropy phase. The use of colloidal nanoparticle cation exchange as a synthetic platform provides both entropic and enthalpic driving forces that, in addition to configurational entropy, enable the formation of high entropy phases at solution-accessible temperatures.

INTRODUCTION

High entropy materials are crystalline solids that typically contain five or more elements, in comparable ratios, randomly distributed throughout a crystal structure.[1] Because high entropy materials incorporate a large number of different elements, they have unique synergistic functions that give rise to useful catalytic,[2,3] electrochemical,[4,5] and mechanical[6] properties. Alloys[2,3,7] and metal oxides[4,5,8] comprise most of the known high entropy materials, although some high entropy metal nitrides,[9] carbides,[10] diborides,[11] halides,[12] and chalcogenides[13,14] are also known. The formation of these high entropy phases is typically driven by their high configurational entropy, which arises from the mixing of the large number of elements.[8] For this entropic driving force to play a prominent role in facilitating the formation of high entropy materials, high temperatures are usually required to maximize the magnitude of the $T\Delta S$ term in the Gibbs free energy equation, often followed by rapid quenching to trap the phase.[8]

Nanostructuring is important for many of the desired applications of high entropy materials, including in catalysis where maximizing surface area maximizes active site density.[15,16] However, strategies for synthesizing nanostructured high entropy materials are limited because of the competing requirements of achieving high configurational entropy, which is facilitated by high-temperature reactions, and preventing particle growth, which is facilitated by low-temperature reactions. Substrate-bound high entropy alloy nanoparticles can be synthesized using a carbothermal shock method, which achieves extremely high temperatures and very rapid heating and cooling rates.[2] Colloidal high entropy alloy nanoparticles can be synthesized using slow injection of dilute metal salt solutions, which preferentially nucleates and grows the high entropy alloy.[3] Capabilities for synthesizing nanoparticles of high entropy materials remain limited, as do the classes of materials for which nanoparticles are available.

Here, we show that colloidal nanoparticles of a high entropy metal sulfide can be synthesized at low temperatures using a conceptually different pathway than those that have been used previously. Starting with roxbyite copper sulfide ($Cu_{1.8}S$) nanoparticles, simultaneous multi-cation exchange with substoichiometric amounts of Zn^{2+}, Co^{2+}, In^{3+}, and Ga^{3+} produces a crystalline, wurtzite-type Zn-Co-In-Ga-Cu sulfide product (Figure 1).

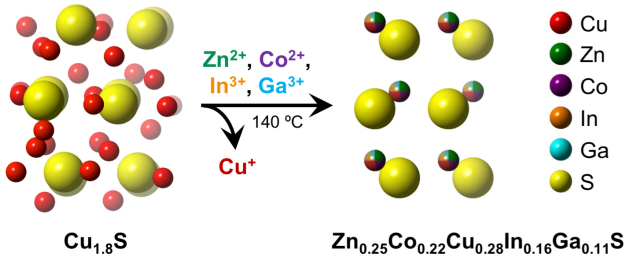

Figure 1. Schematic showing the formation of the high entropy wurtzite-type metal sulfide $Zn_{0.25}Co_{0.22}Cu_{0.28}In_{0.16}Ga_{0.11}S$ from simultaneous Zn^{2+}, Co^{2+}, In^{3+}, and Ga^{3+} exchange of a large fraction (but not all) of the Cu^{+} cations in roxbyite $Cu_{1.8}S$.

There are four unique aspects to this conceptually different approach to producing high entropy materials. First, nanoparticle cation exchange reactions, in which cations in the nanoparticle are replaced by cations from solution, have both enthalpic and entropic driving forces,[17] and these can work together (in addition to configurational entropy) to help drive the formation of a high entropy material at low temperatures. Second, existing approaches to forming high entropy materials involve the direct combination of the constituent elements. Cation exchange, which is a postsynthetic modification strategy, decouples the formation

of the ordered crystal structure and the randomization of the cations. Third, simultaneous exchange of such a large number of cations in colloidal nanoparticles has not been demonstrated. Multi-cation exchange reactions in nanoparticles are either limited to a small number of cations[18,19] or are performed sequentially, which leads to heterostructured products.[20,21] Simultaneous exchange of a large number of cations is fundamentally different, and leads to different products. Fourth, there has only been one report, to our knowledge, of high entropy metal sulfides. $Cu_5SnMgGeZnS_9$ and $Cu_3SnMgInZnS_7$, of interest as thermoelectric materials, were synthesized as bulk solids at high temperatures and pressures using rapid heating and spark plasma sintering.[13] Nanostructured high entropy metal sulfides, which are potentially desirable targets for thermoelectrics, catalysis, and battery materials, have not been reported.

EXPERIMENTAL SECTION

Chemicals. Benzyl ether [99%] was purchased from Acros Organics. Octadecene [ODE, 90%, technical grade], technical grade oleylamine [tg-OLAM, 70%], di-tert-butyl disulfide [97%], copper(II) chloride [$CuCl_2$, 97%], zinc (II) chloride [$ZnCl_2$, ≥ 97% ACS reagent grade, anhydrous], and cobalt(II) chloride [$CoCl_2$, 97%] were purchased from Sigma Aldrich. Indium(III) chloride [$InCl_3$, 98+%, anhydrous] and manganese (II) chloride tetrahydrate [99% trace metal basis] were purchased from Alfa Aesar. Gallium(III) chloride [$GaCl_3$, >98%, anhydrous] and trioctylphosphine [TOP, >85%] were purchased from TCI America. All solvents, including hexanes, isopropanol [IPA], toluene, and acetone, were of analytical grade. All the above chemicals were used as received without further purification. Distilled oleylamine (d-OLAM) was prepared from tg-OLAM, using an established procedure.[21]

Synthesis of $Cu_{1.8}S$ (roxbyite) nanospheres. Roxbyite copper sulfide, $Cu_{1.8}S$, was prepared through a modification of a published procedure.[20] 341 mg of $CuCl_2$, 47.2 mL of d-OLAM, and 11.8 mL of ODE were combined in a 100-mL 3-neck round bottom flask with a magnetic stir bar, reflux condenser, gas flow adapter, alcohol thermometer, and rubber septum. The mixture was placed under vacuum and heated to 100 ºC and held at this temperature for 30 minutes while stirring. The flask is then placed under an Ar flow after cycling the flask between vacuum and Ar three times. The solution was heated to 200 ºC for 1 hour under an Ar flow. The solution was cooled to 180 ºC and 8 mL of di-tertbutyl disulfide (which was under Ar) was rapidly injected. The solution was allowed to re-establish a temperature of 180 ºC, and after 15 min, the flask was placed in a water bath. The product was isolated by adding a 1:1 mixture of IPA and acetone in the brown/black suspension followed by centrifugation and resuspension in toluene. The wash with a 1:1 mixture of IPA and acetone, followed by centrifugation, was repeated two more times for a total of 3 washes. The final brown/black product was suspended in hexanes. The resulting nanoparticles had diameters of approximately 15-20 nm, as seen in Figure S1.

Cation exchange reactions. All the cation exchange reactions were carried out following a modified published protocol.[21,22] The suspension of $Cu_{1.8}S$ nanoparticles in hexanes was added to septum capped vials, and placed under vacuum to remove hexanes. The mass of $Cu_{1.8}S$ was determined by comparing the mass of a vial before and after the suspension was added and the hexanes removed. A typical reaction has approximately 10-20 mg of $Cu_{1.8}S$. Exchange solutions were prepared by dissolving each metal chloride salt in tg-OLAM, ODE, and benzyl ether prior to the reaction; these stock solutions were used for multiple reactions. Table S1 provides the amounts of reagents and solvents used to make the exchange solutions. Based on the starting amount of $Cu_{1.8}S$, the appropriate volume of each exchange solution (described in detail in the Supporting Information) – 0.495 mL for $ZnCl_2$, 0.585 mL for $CoCl_2$, 0.885 mL for $InCl_3$, and 0.780 mL for $GaCl_3$ – was added to a 50 mL round bottom flask equipped with a magnetic stir bar, reflux condenser, gas flow adapter, alcohol thermometer, and rubber septum. Once all the exchange solutions were added, 7.5 mL of benzyl ether, 4 mL of tg-OLAM, and 1 mL of ODE were added to the round bottom flask. Then, this mixture was stirred, placed under vacuum, and heated to 110 ºC for 30 min. Then the reaction mixture was cycled three times with Ar and vacuum and placed under an Ar blanket. Under the Ar blanket, the reaction was heated to 180 ºC and held there for 30 min. In this step, we are preparing a cation–OLAM complex *in situ* as reported previously[20]. During these heating steps, 3 mL of TOP (stored under Ar) was injected into an Ar filled vial containing 15mg $Cu_{1.8}S$ nanospheres. This suspension was cycled twice between vacuum and Ar. The suspension of $Cu_{1.8}S$ nanospheres in TOP (now under Ar) was then sonicated for 45 min. The temperature of the reaction mixture was then decreased to 140 ºC and the suspension of $Cu_{1.8}S$ nanospheres in TOP was rapidly injected. After the reaction returned to 140 ºC, it was held there for 30 min. The reaction mixture was then placed in an ice bath. Once the temperature of the reaction mixture was approx. 10–20 ºC, the reaction mixture was poured into a centrifuge tube, then a 1:1 mixture of IPA and acetone was added, followed by centrifugation and resuspension in toluene. This washing procedure was repeated twice, and the final red/brown product was suspended in hexanes.

Furnace Annealing. Approximately 3 mg of the $Zn_{0.25}Co_{0.22}Cu_{0.28}In_{0.16}Ga_{0.11}S$ nanoparticles suspended in hexanes were dropcast onto a silicon wafer. The silicon wafer was then loaded into a quartz ampoule, which was evacuated to a pressure of 20 mtorr and then flame sealed. The ampoule was then placed in a furnace at room temperature, which was then ramped up (10 °C/min) to 600 ºC and held at that temperature for approximately 24 hours.

Solution Annealing. Approximately 12 mg of $Zn_{0.25}Co_{0.22}Cu_{0.28}In_{0.16}Ga_{0.11}S$ nanoparticles suspended in hexanes was added to a 50 mL round bottom flask equipped with a magnetic stir bar, reflux condenser, gas flow adapter, alcohol thermometer, and rubber septum. 15 mL of ODE was added. The flask was then placed under vacuum at 100 ºC for 30 minutes. The flask was then cycled between vacuum and Ar three times. Now under Ar, the temperature is raised to 300 ºC. The reaction solution was held at this temperature for 5 hours. The reaction was then cooled to room temperature. The reaction mixture was poured into a centrifuge tube, then a 1:1 mixture of IPA and acetone was added, followed by centrifugation and resuspension in hexanes.

Characterization. Transmission electron microscopy (TEM) images (Figure S1) were collected on a FEI Tecnai G20 20 XTWIN microscope operating at 200 kV. High angle annular dark field scanning TEM (HAADF-STEM) and STEM energy dispersive X-ray spectroscopy (STEM-EDS) maps were collected on a FEI Talos F2000X S/TEM at an accelerating voltage of 200 kV. Bruker ESPIRIT 2 software was used to interpret the STEM-EDS element map data. The EDS lines mapped were the Cu Kα, Zn Kα, Co Kα, In Lα, Ga Kα, and S Kα. ImageJ software was used to analyze TEM images. Powder X-ray diffraction (XRD) data were collected on a Bruker D-8 Advance X-ray diffractometer using Cu Kα radiation (Figures S2 and S13), a Malvern PANaltical Empyrean I using Cu Kα radiation (Figure 4, S14, and S16) , and a Malvern PANalytical Empyrean II using Co Kα radiation (Figures 3 and 5). All crystal structures shown were generated using CrystalMaker® and all simulated diffraction patterns were generated using CrystalDiffract®. Both are distributed by CrystalMaker Software Ltd, Oxford, England (www.crystalmaker.com)

RESULTS AND DISCUSSION

We began by choosing four cations to incorporate (Zn^{2+}, Co^{2+}, In^{3+}, Ga^{3+}), in addition to Cu^+ – for a total of five cations – that undergo cation exchange in roxbyite $Cu_{1.8}S$ at similar rates and under similar reaction conditions. Nanocrystal cation exchange reactions proceed based primarily on enthalpic considerations.[17] For example, a soft base such as trioctylphosphine (TOP) in solu-

tion helps to drive the Cu^+ cations, which are soft acids, out of the roxbyite nanocrystals and into solution, where they coordinate with the TOP. This in turn helps to drive the divalent and trivalent cations, which are harder acids, that are initially in solution into the nanocrystal.[17] While cation size does not play a key role, it is noteworthy that all of the cations are similar in size; Cu^+, Zn^{2+}, Co^{2+}, and In^{3+} in tetrahedral coordination environments have ionic radii that are within 0.04 Å of one another, while Ga^{3+} is a bit smaller.[23] Nanocrystal cation exchange of roxbyite $Cu_{1.8}S$ with each of the individual cations is well known. The products of Zn^{2+} and Co^{2+} exchange of roxbyite $Cu_{1.8}S$ are wurtzite ZnS[24] and wurtzite CoS,[25] respectively; both reactions release two equivalents of Cu^+ for every one equivalent of divalent cation that is incorporated into the nanocrystal. The products of In^{3+} and Ga^{3+} cation exchange are wurtzite $CuInS_2$[24] and wurtzite $CuGaS_2$,[21] respectively. Here, three Cu^+ cations are released for every trivalent cation that is exchanged, but some Cu^+ from the roxbyite remains in the final $CuInS_2$ and $CuGaS_2$ products. $Cu_{1.8}S$ has been shown in one case to transform to Cu_2S *in situ* prior to initiation of cation exchange.[26] Charge is therefore considered to be balanced in these reactions, although the products are likely defect-rich.

Given this knowledge of nanocrystal cation exchange chemistry, we targeted a wurtzite-type high entropy metal sulfide consisting of an equimolar solid solution of ZnS, CoS, $CuInS_2$, and $CuGaS_2$. Stock solutions of $ZnCl_2$, $CoCl_2$, $InCl_3$, and $GaCl_3$ in oleylamine, octadecene, and benzyl ether were prepared, and precise volumes of these solutions, corresponding to substoichiometric amounts of each cation relative to the amount of Cu^+ in the $Cu_{1.8}S$ nanoparticles, were combined in a separate flask with additional oleylamine, octadecene, and benzyl ether. The molar ratios were chosen to retain some of the original Cu^+, as discussed above, and to generate a product having ¼ ZnS, ¼ CoS, ¼ $CuInS_2$, and ¼ $CuGaS_2$, which corresponds to a nominal composition of $Zn_{0.25}Co_{0.25}Cu_{0.25}In_{0.125}Ga_{0.125}S$. The solution containing four metal salts was placed under vacuum, heated to 100 °C, and held there for 30 minutes. After three cycles of vacuum and Ar purging, the solution was heated to 180 °C under Ar, held for 30 minutes, cooled to 140 °C, and then a suspension of the $Cu_{1.8}S$ nanoparticles dispersed in trioctylphosphine was injected. The reaction was then allowed to proceed for 30 minutes before isolating the product, which was found to form reproducibly.

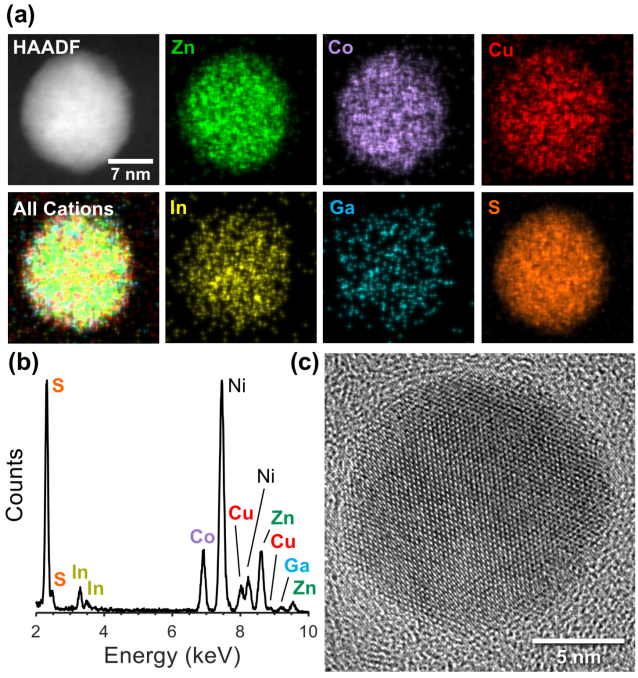

Figure 2. Microscopic characterization of a single $Zn_{0.25}Co_{0.22}Cu_{0.28}In_{0.16}Ga_{0.11}S$ nanoparticle: (a) HAADF-STEM image and corresponding STEM-EDS element maps (Cu Kα, Zn Kα, Co Kα, In Lα, Ga Kα, S Kα), along with an overlaid image; (b) EDS spectrum; and (c) HRTEM image. The Ni signal in (b) comes from the Ni TEM grid.

A HAADF-STEM image and corresponding STEM-EDS element maps for a single particle from the isolated product is shown in Figure 2a; wider-view images and element maps are shown in Figure S3. The STEM-EDS maps show that Zn, Co, Cu, In, Ga, and S are all present and uniformly distributed within the particles. An EDS spectrum obtained from a larger ensemble of particles, shown in Figure S4, indicates an approximate composition of $Zn_{0.25}Co_{0.22}Cu_{0.28}In_{0.16}Ga_{0.11}S$, which matches well with the expected composition. Table S2 provides an error analysis for this composition. Assuming the formation of a single-phase wurtzite-type high entropy metal sulfide having the composition determined by EDS analysis, the lattice parameters can be estimated using a weighted average of those of the constituent wurtzite phases. Using this approach, which is described in detail in the Supporting Information, the lattice parameters for wurtzite-type $Zn_{0.25}Co_{0.22}Cu_{0.28}In_{0.16}Ga_{0.11}S$ are expected to be a = 3.81 Å and c = 6.28 Å. Figure 2c shows a HRTEM image of a $Zn_{0.25}Co_{0.22}Cu_{0.28}In_{0.16}Ga_{0.11}S$ particle, confirming that it retains the single crystalline nature of the precursor $Cu_{1.8}S$ nanoparticles.

The XRD pattern (Figure 3) is consistent with a single-phase nanocrystalline wurtzite product; no crystalline impurities were observed by XRD and no amorphous components were observed microscopically. Scherrer analysis of peak widths indicate an average crystalline domain size of 13 nm, which is on par with the average particle sizes observed in Figures 2 and S3 and the knowledge from the HRTEM image that the particles are single crystalline. Figure 3 also shows a simulated XRD pattern that was generated by randomly distributing Zn, Co, Cu, In, and Ga on the metal sites of a wurtzite-type sulfide crystal structure, with the cation ratios matching the experimentally observed molar ratios. The simulated XRD pattern uses the estimated lattice parameters described above. The good match between the experimental and simulated XRD patterns validates the formation of nanoparticles of the high entropy sulfide $Zn_{0.25}Co_{0.22}Cu_{0.28}In_{0.16}Ga_{0.11}S$.

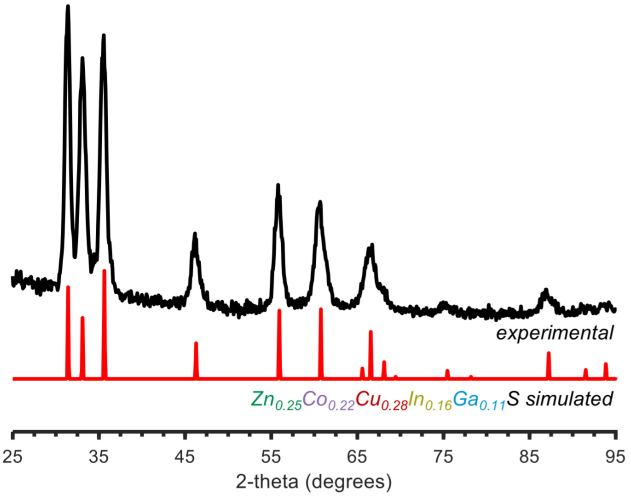

Figure 3. Experimental and simulated XRD patterns (using Co Kα radiation) for a powder sample of the wurtzite-type $Zn_{0.25}Co_{0.22}Cu_{0.28}In_{0.16}Ga_{0.11}S$ nanoparticles. Details about how the simulated pattern was generated are included in the Supporting Information.

Our initial focus was on $Zn_{0.25}Co_{0.22}Cu_{0.28}In_{0.16}Ga_{0.11}S$, which represents an equimolar, substoichiometric loading of Zn^{2+}, Co^{2+}, In^{3+}, and Ga^{3+} reagents. However, it is important to be able to tune the stoichiometry and composition of high entropy materials, as these can impact the properties, such as in catalysis.[15] We

therefore explored the formation of other stoichiometries within the Zn–Co–Cu–In–Ga–S system, keeping in mind the need to maintain charge balance. We targeted four stoichiometries that contained 40% of one of the constituent metal sulfides and 20% of the others. This included samples that were (relative to the initial targeted stoichiometry of $Zn_{0.25}Co_{0.25}Cu_{0.25}In_{0.125}Ga_{0.125}S$) Co-rich ($Zn_{0.2}Co_{0.4}Cu_{0.2}In_{0.1}Ga_{0.1}S$), Zn-rich ($Zn_{0.4}Co_{0.2}Cu_{0.2}In_{0.1}Ga_{0.1}S$), In-rich ($Zn_{0.2}Co_{0.2}Cu_{0.3}In_{0.2}Ga_{0.1}S$), and Ga-rich ($Zn_{0.2}Co_{0.2}Cu_{0.3}In_{0.1}Ga_{0.2}S$). The XRD patterns for each of these samples, shown in Figure 4, are consistent with single-phase wurtzite compounds. The lattice parameters, included in Table S4 of the Supporting Information, show subtle but measurable shifts that are qualitatively consistent with the targeted stoichiometry differences. Table S4 also summarizes the initial cation stoichiometries in solution and the experimentally determined cation stoichiometries in the products. EDS data, including images and compositions, are shown in Figure S6-S9 of the Supporting Information. Like the initial system, all of the stoichiometry-tuned systems exhibit uniform mixing of all cations throughout the nanoparticles. Additionally, the EDS composition matches qualitatively with the targeted composition, indicating that the stoichiometry of the high-entropy metal sulfide nanoparticles can be tuned simply by adjusting the ratios of exchanging cations in solution. A preliminary experiment hints that it may also be possible to substitute other cations to target different compositions, *i.e.* the Zn–Mn–Cu–In–Ga–S system in Figure S10.

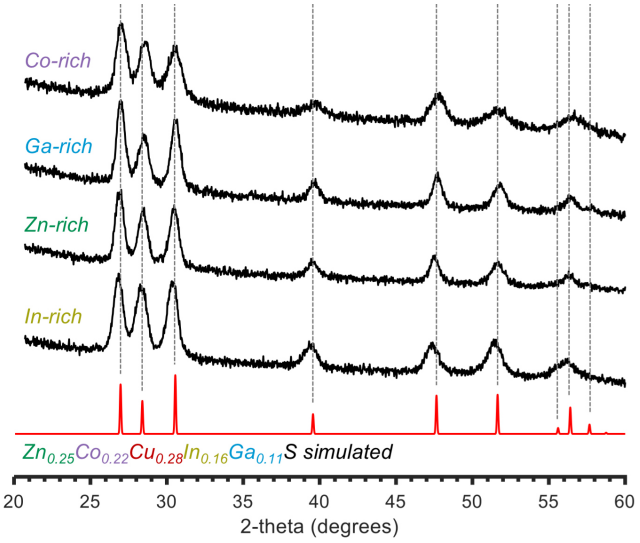

Figure 4. XRD patterns (using Cu Kα radiation) corresponding to products obtained using different ratios of cation exchange solution. In-rich, Zn-rich, Ga-rich, and Co-rich compositions (relative to the initial targeted stoichiometry of $Zn_{0.25}Co_{0.25}Cu_{0.25}In_{0.125}Ga_{0.125}S$, and as described in the text) are shown. The simulated pattern for a $Zn_{0.25}Co_{0.22}Cu_{0.28}In_{0.16}Ga_{0.11}S$ pattern is shown for reference.

For high entropy phases to form, a large number of randomly distributed elements (typically 5 or more) must be present, as this is generally required to yield a sufficiently high configurational entropy term. As a result, it is commonly observed in bulk high entropy material systems that smaller subsets of those same elements do not yield single-phase solid solutions, but rather produce samples that contain multiple segregated phases. For example, in the bulk, high-temperature synthesis of $Mg_{0.2}Co_{0.2}Cu_{0.2}Ni_{0.2}Zn_{0.2}O$, removing any metal oxide reactant fails to produce a solid solution under the same reaction conditions; mixed phase products are observed instead.[8] To probe analogous behavior in our high entropy metal sulfide nanoparticles made through cation exchange, we carried out control experiments involving simultaneous exchange with smaller numbers of cations. Figure 5 shows the XRD pattern for the product obtained through simultaneous cation exchange using Zn^{2+} and In^{3+}, which represents a 3-cation system (Zn^{2+}, In^{3+}, Cu^{+}). Asymmetric peaks, along with peak splitting at high angles, is consistent with a two-phase sample, indicating that the attempted Zn-In-Cu sulfide does not form a complete solid solution. Simultaneous Zn^{2+}, Co^{2+}, and In^{3+} exchange, in an attempt to produce a 4-cation (Zn^{2+}, Co^{2+}, In^{3+}, Cu^{+}) sulfide, is similarly consistent with a multi-phase sample, based on the peak shape and splitting (Figure 5). Both XRD patterns differ significantly from that of the single-phase, equimolar Zn-Co-Cu-In-Ga sulfide, also shown in Figure 5 for comparison. The phase formation behavior at low temperatures in our metal sulfide system synthesized using simultaneous multi-cation exchange is therefore analogous to that of bulk high entropy phases formed using direct high-temperature methods.

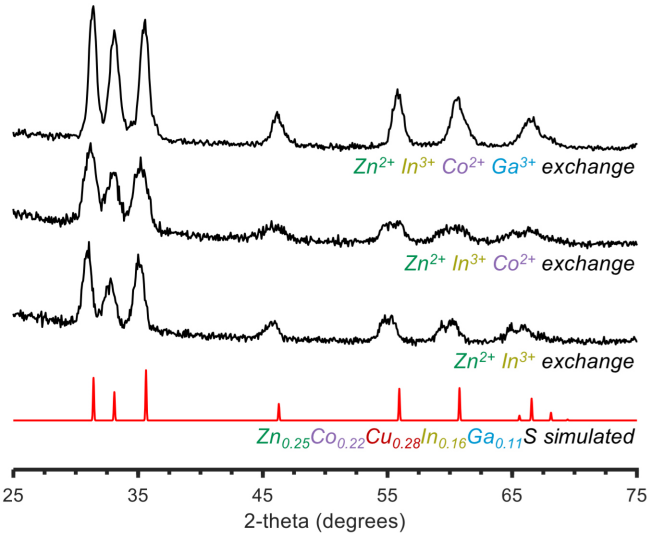

Figure 5. XRD patterns (using Co Kα radiation) corresponding to products obtained using different numbers of simultaneously exchanged cations. Exchanges with two and three cations produced mixtures of products, while exchange with four cations produced the high entropy phase. The top XRD pattern and simulated $Zn_{0.25}Co_{0.22}Cu_{0.28}In_{0.16}Ga_{0.11}S$ pattern, shown for comparison, are duplicated from Figure 3.

Additional control experiments provide further insights into the stability of the high entropy metal sulfide nanoparticles. First, when the $Zn_{0.25}Co_{0.22}Cu_{0.28}In_{0.16}Ga_{0.11}S$ nanoparticles, which were synthesized at 140 °C, were annealed at 300 °C in octadecene, the high entropy phase was retained (Figure S13). Second, when the $Zn_{0.25}Co_{0.22}Cu_{0.28}In_{0.16}Ga_{0.11}S$ nanoparticles were heated as a powder in a sealed evacuated ampoule at 600 °C, they also remained as a high entropy phase (Figure S14). These results confirm that, once formed, the phase persists at significantly higher temperatures.

The formation of bulk high entropy materials at high temperatures is typically attributed to the high configurational entropy that results from the random distribution of atoms in a crystalline lattice. To rationalize the formation of our high entropy sulfide made through nanoparticle cation exchange, we must consider a broader scope of both enthalpic and entropic contributions. Enthalphic contributions from solution-phase processes such as solvation of the Cu^{+} by TOP to drive the exchange reaction, which are not present in typical solid-state reactions (*i.e.* those that are typically used to synthesize high entropy materials), are significant drivers of spontaneous cation exchange reactions in colloidal nanoparticles.[17] The competition between solid solution formation vs heterostructuring must also be considered, as nanopar-

ticle cation exchange reactions can sometimes generate products with phase-segregated regions connected through interfaces. Interface formation within a particle resulting from phase segregation during cation exchange constitutes an enthalpic penalty that would increase in magnitude as the number of exchanging cations, and concomitantly the number of interfaces, increases. Entropic driving forces can also be significant, as two or three Cu^{+} cations are released into solution for every M^{2+} or M^{3+} cation, respectively, that enters the nanocrystal. At the same time, by separating the cation randomization step from the ordered crystal lattice formation step, as is the case for this post-synthetic modification strategy, the configurational entropy remains significant. A full treatment of the thermodynamics of these processes would need to quantitatively consider all relevant factors and also account for size-dependent phenomena.[18,19] However, it is clear that the unique aspects of nanoparticle cation exchange modify the driving forces and offer a conceptually different reaction pathway to the formation of high entropy materials.

To provide a glimpse of how the high entropy metal sulfide nanoparticles form through simultaneous multi-cation exchange of roxbyite copper sulfide, we quenched a reaction after it had proceeded for only one minute; note that the full reaction time used for all samples was 30 minutes. Figures 6 and S15 show HAADF-STEM images and STEM-EDS element maps of the particles isolated from this reaction that had been quenched after one minute. Even at this early time point, most of the particles appear to be the high-entropy metal sulfide, *i.e*. the simultaneous cation exchange reaction happened almost immediately and nearly went to completion. This is evident in both the STEM-EDS images as well as XRD (Figure S16). However, in all regions that were imaged, a few Janus particles were found. These Janus particles had one hemisphere of copper sulfide and one hemisphere of the high entropy metal sulfide. Importantly, we did not observe any regions where other multi-cation sulfides were present, *i.e*. there was not any evidence of 2-, 3-, or 4-cation metal sulfides, only a 5-cation metal sulfide and the starting $Cu_{1.8}S$. The data therefore suggest that the cation exchange process that generates the high-entropy metal sulfide proceeds as expected, where all cations are replaced simultaneously in the regions they ultimately inhabit and diffuse through the crystal, rather than by stepwise diffusion processes or interdiffusion of phase segregated regions. This behavior is analogous to well-studied cation exchange reactions that transform copper sulfide nanocrystals into targeted binary and ternary phases.[17]

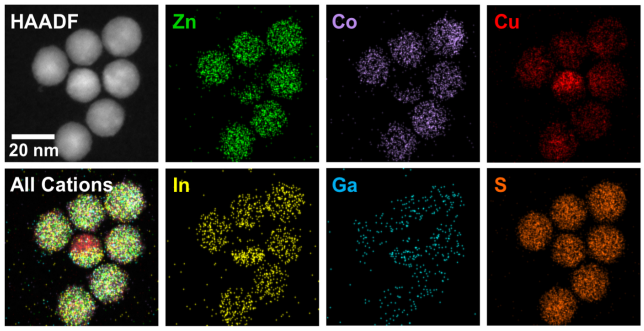

Figure 6. HAADF-STEM image and corresponding STEM-EDS element maps (Cu Kα, Zn Kα, Co Kα, In Lα, Ga Kα, S Kα), along with an overlaid image, for a simultaneous Zn^{2+}, Co^{2+}, In^{3+}, and Ga^{3+} cation exchange quenched one minute into the 30-minute reaction. All particles, except one, are completely exchanged. The partially exchanged particle has a $Cu_{2-x}S$ hemisphere and a Zn-Co-Cu-In-Ga-S hemisphere.

CONCLUSIONS

In conclusion, we have introduced simultaneous multi-cation exchange as a postsynthetic modification strategy to access colloidal nanoparticles of a high entropy metal sulfide at low temperatures. The stoichiometry can be tuned by adjusting the ratios of exchanging cations in solution. The cation exchange process that forms the high entropy material is believed to be both entropically and enthalpically favored and also separates the formation of an ordered structure from the randomization of cations. This provides a new approach to designing and synthesizing high entropy materials that is likely to be extendable to other systems that are amenable to cation exchange, including metal selenides,[27] metal tellurides,[28] metal phosphides,[29] and metal halides.[30] This approach also offers a pathway toward nanostructuring that is anticipated to be of interest for applications in catalysis, energy storage, and thermoelectrics.

ASSOCIATED CONTENT

Supporting Information

The Supporting Information is available free of charge on the ACS Publications website.

Complete synthetic methods, additional XRD and TEM characterization, details on compositional analysis and simulated XRD pattern, and references which provide lattice parameters for each respective sulfide (31-34).

AUTHOR INFORMATION

Corresponding Author

*res20@psu.edu

Notes

The authors declare no competing financial interests.

ACKNOWLEDGMENT

This work was supported by the U.S. National Science Foundation under grant DMR-1904122. TEM imaging and X-ray diffraction were performed at the Materials Characterization Lab of the Penn State Materials Research Institute.

REFERENCES

(1) Yeh, J. W.; Chen, S. K.; Lin, S. J.; Gan, J. Y.; Chin, T. S.; Shun, T. T.; Tsau, C. H.; Chang, S. Y. Nanostructured High-Entropy Alloys with Multiple Principal Elements: Novel Alloy Design Concepts and Outcomes. *Adv. Eng. Mater.* **2004**, *6*, 299–303.

(2) Yao, Y.; Huang, Z.; Xie, P.; Lacey, S. D.; Jacob, R. J.; Xie, H.; Chen, F.; Nie, A.; Pu, T.; Rehwoldt, M.; Yu, D.; Zachariah, M.R.; Wang, C.; Shahbazian-Yassar, R.; Li, J.; Hu, L. Carbothermal Shock Synthesis of High-Entropy-Alloy Nanoparticles. *Science* **2018**, *359*, 1489–1494.

(3) Wu, D.; Kusada, K.; Yamamoto, T.; Toriyama, T.; Matsumura, S.; Kawaguchi, S.; Kubota, Y.; Kitagawa, H. Platinum-Group-Metal High-Entropy-Alloy Nanoparticles. *J. Am. Chem. Soc.* **2020**, *142*, 13833–13838.

(4) Sarkar, A.; Velasco, L.; Wang, D.; Wang, Q.; Talasila, G.; de Biasi, L.; Kübel, C.; Brezesinski, T.; Bhattacharya, S. S.; Hahn, H.; Breitung, B. High Entropy Oxides for Reversible Energy Storage. *Nat. Commun.* **2018**, *9*, 3400.

(5) Zhao, C.; Ding, F.; Lu, Y.; Chen, L.; Hu, Y. High-Entropy Layered Oxide Cathodes for Sodium-Ion Batteries. *Angew. Chem., Int. Ed.* **2020**, *59*, 264–269.

(6) Gludovatz, B.; Hohenwarter, A.; Catoor, D.; Change, E. H.; George, E. P.; Ritchie, R. O. A Fracture-Resistant High-Entropy Alloy for Cryogenic Applications. *Science* **2014**, *345*, 1153–1158.

(7) George, E. P.; Raabe, D.; Ritchie, R. O. High-Entropy Alloys. *Nat. Rev. Mater.* **2019**, *4*, 515–534.

(8) Rost, C. M.; Sachet, E.; Borman, T.; Moballegh, A.; Dickey, E. C.; Hou, D.; Jones, J. L.; Curtarolo, S.; Maria, J. P. Entropy-Stabilized Oxides. *Nat. Commun.* **2015**, *6*, 8485.

(9) Hsieh, M. H.; Tsai, M. H.; Shen, W. J.; Yeh, J. W. Structure and Properties of Two Al-Cr-Nb-Si-Ti High-Entropy Nitride Coatings. *Surf. Coatings Technol.* **2013**, *221*, 118–123.

(10) Castle, E.; Csanádi, T.; Grasso, S.; Dusza, J.; Reece, M. Processing and Properties of High-Entropy Ultra-High Temperature Carbides. *Sci. Rep.* **2018**, *8*, 8609.

(11) Gild, J.; Zhang, Y.; Harrington, T.; Jiang, S.; Hu, T.; Quinn, M. C.; Mellor, W. M.; Zhou, N.; Vecchio, K.; Luo, J. High-Entropy Metal Diborides: A New Class of High-Entropy Materials and a New Type of Ultrahigh Temperature Ceramics. *Sci. Rep.* **2016**, *6*, 37946.

(12) Wang, T.; Chen, H.; Yang, Z.; Liang, J.; Dai, S. High-Entropy Perovskite Fluorides: A New Platform for Oxygen Evolution Catalysis. *J. Am. Chem. Soc.* **2020**, *142*, 4550–4554.

(13) Zhang, R. Z.; Gucci, F.; Zhu, H.; Chen, K.; Reece, M. J. Data-Driven Design of Ecofriendly Thermoelectric High-Entropy Sulfides. *Inorg. Chem.* **2018**, *57*, 13027–13033.

(14) Deng, Z.; Olvera, A.; Casamento, J.; Lopez, J. S.; Williams, L.; Lu, R.; Shi, G.; Poudeu, P. F. P.; Kioupakis, E. Semiconducting High-Entropy Chalcogenide Alloys with Ambi-Ionic Entropy Stabilization and Ambipolar Doping. *Chem. Mater.* **2020**, *32*, 6070–6077.

(15) Löffler, T.; Savan, A.; Garzón-Manjón, A.; Meischein, M.; Scheu, C.; Ludwig, A.; Schuhmann, W. Toward a Paradigm Shift in Electrocatalysis Using Complex Solid Solution Nanoparticles. *ACS Energy Lett.* **2019**, *4*, 1206–1214.

(16) Koo, W.-T.; Millstone, J. E.; Weiss, P. S.; Kim, I.-D. The Design and Science of Polyelemental Nanoparticles. *ACS Nano* **2020**, *14*, 64017–66413.

(17) De Trizio, L.; Manna, L. Forging Colloidal Nanostructures via Cation Exchange Reactions. *Chem. Rev.* **2016**, *116*, 10852–10887.

(18) Akkerman, Q. A.; Genovese, A.; George, C.; Prato, M.; Moreels, I.; Casu, A.; Marras, S.; Curcio, A.; Scarpellini, A.; Pellegrino, T.; Manna, L.; Lesnnyak, V. From Binary Cu_2S to Ternary Cu-In-S and Quaternary Cu-In-Zn-S Nanocrystals with Tunable Composition via Partial Cation Exchange. *ACS Nano* **2015**, *9*, 521–531.

(19) Flanagan, J. C.; Keating, L. P.; Kalasad, M. N.; Shim, M. Extending the Spectral Range of Double-Heterojunction Nanorods by Cation Exchange-Induced Alloying. *Chem. Mater.* **2019**, *31*, 9307–9316.

(20) Fenton, J. L.; Steimle, B. C.; Schaak, R. E. Tunable Intraparticle Frameworks for Creating Complex Heterostructured Nanoparticle Libraries. *Science* **2018**, *360*, 513–517.

(21) Steimle, B. C.; Fenton, J. L.; Schaak, R. E. Rational Construction of a Scalable Heterostructured Nanorod Megalibrary. *Science* **2020**, *367*, 418–424.

(22) Steimle, B. C.; Fagan, A. M.; Butterfield, A. G.; Lord, R. W.; McCormick, C. R.; Di Domizio, G. A.; Schaak, R. E. Experimental Insights into Partial Cation Exchange Reactions for Synthesizing Heterostructured Metal Sulfide Nanocrystals. *Chem. Mater.* **2020**, *32*, 5461–5482.

(23) Shannon R. D.; Prewitt, C. T.; Effective Ionic Radii in Oxides and Fluorides. *Acta Crystallogr., Sect B.* **1969**, *25*, 925-946.

(24) Fenton, J. L.; Steimle, B. C.; Schaak, R. E. Structure-Selective Synthesis of Wurtzite and Zincblende ZnS, CdS, and $CuInS_2$ Using Nanoparticle Cation Exchange Reactions. *Inorg. Chem.* **2019**, *58*, 672–678.

(25) Powell, A. E.; Hodges, J. M.; Schaak, R. E. Preserving Both Anion and Cation Sublattice Features during a Nanocrystal Cation-Exchange Reaction: Synthesis of Metastable Wurtzite-Type CoS and MnS. *J. Am. Chem. Soc.* **2016**, *138*, 471–474.

(26) Steimle, B. C.; Lord, R. W.; Schaak, R. E. Phosphine-Induced Phase Transition in Copper Sulfide Nanoparticles Prior to Initiation of a Cation Exchange Reaction. *J. Am. Chem. Soc.* **2020**, *142*, 13345–13349.

(27) Li, H.; Zanella, M; Genovese, A.; Povia, M.; Falqui, A.; Giannini, C.; Manna, L. Sequential Cation Exchange in Nanocrystals: Preservation of Crystal Phase and Formation of Metastable Phases. *Nano Letters*. **2011**, *11*, 4964 - 4970.

(28)Li, H.; Brescia, R.; Povia, M.; Prato, M.; Bertoni, G.; Manna, L.; Moreels, I. Synthesis of Uniform Disk-Shaped Copper Telluride Nanocrystals and Cation Exchange to Cadmium Telluride Quantum Disks with Stable Red Emission. *J. Am. Chem. Soc.*, **2012**, *135*, 12270-12278.

(29)De Trizio, L.; Gaspari, R.; Bertoni, G.; Kriegel, I.; Moretti, L.; Scotognella, F.; Maserati, L.; Zhang, Y.; Messina, G. C.; Prato, M.; Marras, S.; Cavalli, A.; Manna, L. $Cu_{3-x}P$ Nanocrystals as a Material Platform for Near-Infrared Plasmonics and Cation Exchange Reactions. *Chem. Mater.* **2015**, *27*, 1120-1128.

(30) Van der Stam, W.; Geuchies, J. J.; Altantzis, T.; Van Den Bos, K. H. W.; Meeldijk, J. D.; Van Aert, S.; Bals, S.; Vanmaekelbergh, D.; de Mello Donega, C. Highly Emissive Divalent-Ion-Doped Colloidal $CsPb_{1-x}MxBr_3$ Perovskite Nanocrystals through Cation Exchange. *J. Am. Chem. Soc.* **2017**, *139*, 4087–4097.

Table of Contents artwork